Fluids at electrode/membrane interfaces suppress alcohol crossover in CO electroreduction

Haoxiang Bai[1,2], Jundong Wang[1,2], Yuhang Wang[1,*]

[1]*Institute of Functional Nano & Soft Materials (FUNSOM), Soochow University, 199 Ren'ai Road, Suzhou, Jiangsu, 215123, China.*

[2]*These authors contributed equally to this work.*

[*]Correspondence should be addressed to Yuhang Wang (*yhwang1988@suda.edu.cn*).

Experimental section

Synthesis of Cu_2O Nanoparticles

Cu_2O nanocrystals were synthesized via a modified liquid-phase reduction method. First, a 1.2 M Cu^{2+} precursor solution was prepared by dissolving 9.6 g of $CuSO_4 \cdot 5H_2O$ (Meryer, ≥99.99%) in 50 mL deionized (DI) water. Separately, 9.7 g of sodium citrate (Sinopharm Chemical Reagent Co., Ltd., 98%) was dissolved in 50 mL of DI water to prepare a 0.75 M complexing agent solution. The sodium citrate solution was transferred to a 250 mL round-bottom flask under constant stirring (600 rpm) at 20°C. Subsequently, 50 mL of the Cu^{2+} precursor solution was rapidly injected into the flask. After 5 min of mixing, 50 mL of 4.8 M KOH solution (prepared by dissolving 13.5 g KOH in 50 mL DI water) was added dropwise, resulting in a turbid blue suspension indicative of $Cu(OH_2^-$ complex formation. Next, 50 mL of 1.2 M ascorbic acid solution (prepared by dissolving 10.6 g ascorbic acid (Sinopharm Chemical Reagent Co., Ltd., AR grade) in 50 mL DI water) was added, and stirring was continued for 30 min. The solution transitioned from blue to orange, confirming the reduction of Cu^{2+} to Cu_2O nanocrystals. The suspension was centrifuged at 8000 rpm to collect the precipitate, which was washed three times with DI water to remove residual ions and vacuum-dried at 60°C for 12 h to yield orange-red Cu_2O nanopowder.

Morphological and structural characterizations were performed using scanning electron microscopy (Hitachi, Regulus SU8230) and X-ray diffraction (XRD, PANalytical X'Pert Pro).

Electrode Fabrication

CO Reduction Reaction (CORR) Electrode: Gas diffusion electrodes (GDEs) were fabricated by depositing a Cu_2O catalyst layer. A catalyst ink was prepared by dispersing 15 mg of Cu_2O nanopowder in 2 mL of n-propanol, followed by adding 20 μL of Nafion D521 ionomer (DuPont, 5 wt% solution) and sonicating for 30 min to ensure homogeneity. The ink was uniformly coated onto a hydrophobic carbon paper substrate (Avcarb MB30, 2.3 × 2.3 cm^2) to achieve a catalyst loading of ~0.75 mg/cm^2. The electrode was stored in an argon-filled glovebox prior to use.

Catalyst-coated membranes (CCM) Fabrication: Identical GDE catalyst inks were spray-coated directly onto a dry FAA-3-50 membrane (5 × 5 cm^2), followed by immersion in 1 M KOH solution to convert the ionic groups to OH^- form, making the assembly ready for electrolyzer integration.

Oxygen Evolution Reaction (OER) Electrode: A $NiFeO_x$ catalyst was electrodeposited on a nickel foam substrate (2.3 × 2.3 cm^2, Suzhou Suke Lean Instrument Co., Ltd.). The nickel foam was immersed in an aqueous solution containing 3 mM $Ni(NO_{322}\cdot 6H_2O$ (Sinopharm Chemical Reagent Co., Ltd., AR grade) and 3 mM $Fe(NO_3)_3\cdot 9H_2O$ (Macklin, 99.9%). Electrodeposition was conducted in a three-electrode system using a potentiostat (DH7000, Donghua Analytical Instruments), with a platinum wire as the counter electrode and an Ag/AgCl reference electrode. A constant potential of −1.0 V (vs. Ag/AgCl) was applied for 5 min. The resulting NiFe alloy was ultrasonically cleaned in acetone and DI water to obtain the $NiFeO_x$ OER anode.

Membrane Electrode Assembly

A 5 cm^2 rectangular flow-cell electrolyzer was assembled by sequentially stacking the cathode GDE, a pre-activated anion exchange membrane, a gasket, the NiFeOx anode, and a titanium current collector. The components were clamped symmetrically using hexagonal bolts. CO gas (99.99% purity) was fed to the cathode at 40 sccm via a mass flow controller, while 1 M KOH electrolyte was circulated through the anode using a peristaltic pump (Huiyu Weiye Fluid Equipment Co., Ltd.), establishing a gas-liquid-solid triple-phase interface.

With the fluid at the cathode/membrane interface

To enhance mass transport regulation, the conventional design was modified by integrating symmetric DI water circulation channels. A 50 mL sealed buffer chamber was attached to the cathode plate, connected via a four-port manifold: Port 1 delivered DI water via a peristaltic pump, Port 2 supplied CO reactant gas (40 sccm), Port 3 directed the fluid to the cathode channel for hydraulic scouring and reactant co-feeding, and Port 4 interfaced with online gas chromatography for real-time product monitoring. All other assembly steps matched the conventional MEA.

Electrochemical CORR Testing

Electrochemical performance was evaluated via an electrochemical workstation under iR-uncompensated conditions. After stabilizing the cell voltage, the gaseous products from the cathode were analyzed using a gas chromatograph (GC2060, Wuhao Information Technology) equipped with a thermal conductivity detector (TCD) and a flame ionization detector (FID). Product concentrations were quantified via calibration curves derived from standard gases. Total gas flow rates were monitored using a mass flow meter (CS200A, Seven Star Fluid). Faradaic efficiencies (FEs) for gaseous products were calculated as:

$$FE_i(\%) = \frac{Q_i}{Q_{tot}} \times 100\% = \frac{\left(\frac{v}{60\ s/min}\right) \times \left(\frac{y}{24500\ cm^3/mol}\right) \times N \times F \times 100\%}{j}$$

Where v is the gas flow rate at the cathode outlet, y is the measured product concentration in the 1 mL sample loop based on the standard calibration curve, N is the number of electrons transferred in the reaction, F is the Faraday constant (96485 C·mol^{-1}), and j is the total current.

Liquid products were analyzed by high-performance liquid chromatography (HPLC, UltiMate 3000). Their FEs were determined using:

$$FE_i(\%) = m_i \times \frac{N \times F}{j \times t}$$

Where m_i is the amount of liquid products in moles, and t is the duration of the measured product, N is the number of electrons transferred in the reaction, F is the Faraday constant (96485 C·mol^{-1}), and j is the total current.

Product distribution and relative purity are further assessed via:

$$FE\ distribution = \frac{FE_{i,chamber}}{FE_{i,total}}$$

Where $FE_{i,chamber}$ represents the Faradaic efficiency of product i in either the cathode or anode chamber, and $FE_{i,total}$ denotes the total Faradaic efficiency of the same product across the full-cell system.

$$Relative\ purity = \frac{n_i}{n_{total}}$$

Where n_i and n_{total} represent the concentration of product and the sum of all detected products, respectively.

During the long-term test, brief electrolyte management (vial replacement) and momentary gas flow variations occurred but did not disrupt electrolysis.

The effective migration rate of liquid products is calculated via:

$$Effective\ Migration\ Rate\ of\ liquid\ products = \frac{\Delta C_i \times V}{I \times t}$$

Where ΔC_{ace} is product concentration, V is cathode volume, I is applied current, and t is time. The effective migration rate of liquid products is tested under no CO-free conditions.

Product concentration is determined via:

$$Product\ concentration = \frac{m_i \times Mr_i}{m}$$

Where m_i is the amount of liquid product in moles, Mr_i is the relative molecular weight of the product, and m is the mass of the total circulating pure water collected on the cathode side.

Flushing capacity is calculated via:

$$Flushing\ capacity = U_{vertical} \times h_{eff}$$

Where $U_{vertical}$ is the vertical flow rate (cm/s), h_{eff} is the effective interlayer thickness.

Vertical flow rate is calculated via:

$$Vertical\ flow\ rate = \frac{Q}{w \times h_{eff}}$$

Where Q is the total circulating water flow rate at the cathode, h_{eff} is the effective interlayer thickness, w is the width of the flow channel on the cathode plate.

Water uptake measurement

Commercial anion exchange membranes were used as received: FAA-3-20, FAA-3-50, and FAS-50 were acquired from FUMATECH BWT GmbH. PiperION A20, PiperION A40, and PiperION A80 were obtained from Versogen™. H60 was sourced from Suzhou Zhiqing Bocai Technology Co., Ltd.

Anion-exchange membranes in the OH^- form were vacuum-dried at 60°C for 24 hr and weighed to obtain the dry mass (W_d). The dried membranes were immersed in deionized water for 24 h. Surface moisture was removed by tissue paper prior to measuring the hydrated mass (W_w). Water uptake (WU) was calculated as:

$$WU\ (\%) = \frac{W_w - W_d}{W_d} \times 100\%$$

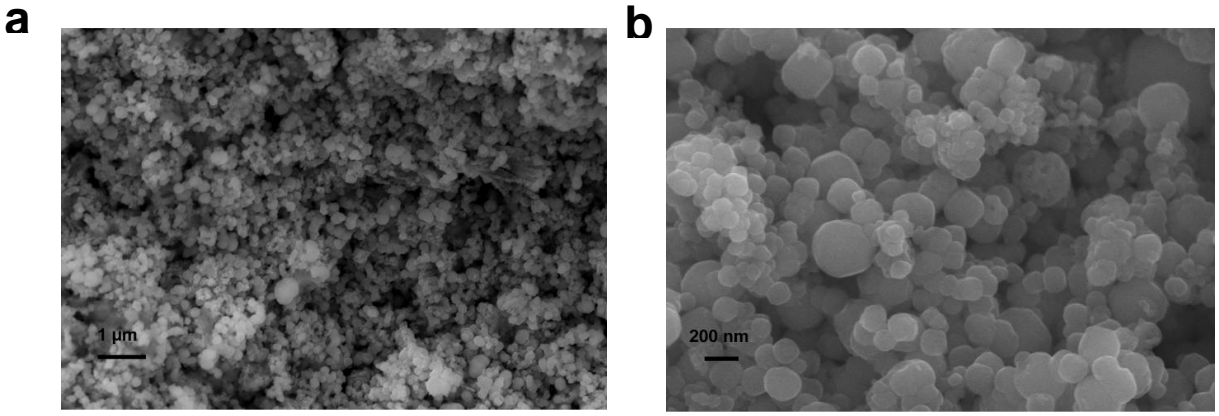

Fig. S1 Morphological characterization of Cu_2O (a) The SEM image of Cu_2O at 1-µm resolution and (b) The SEM image of Cu_2O particles at 200-nm resolution.

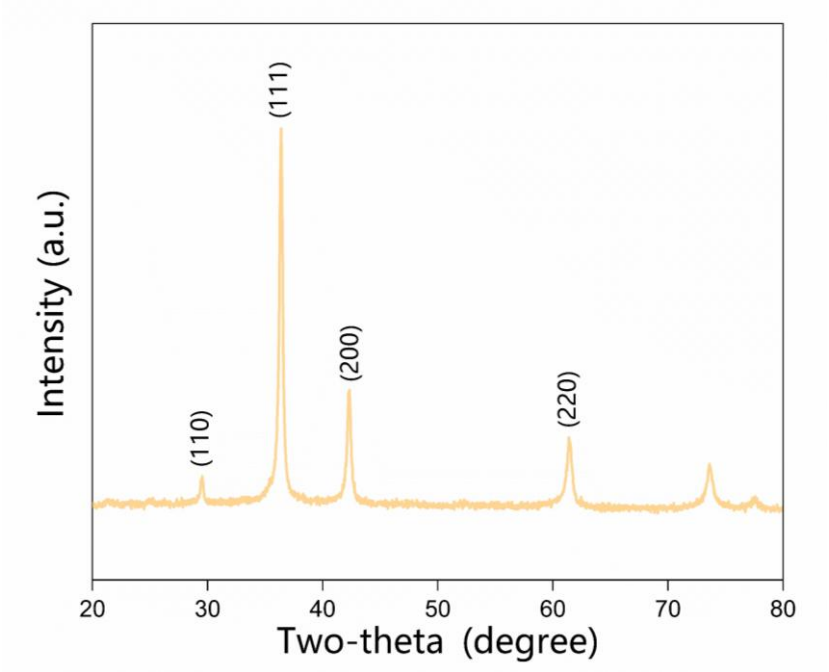

Fig. S2 The XRD pattern of the as-synthesized Cu_2O nanoparticles.

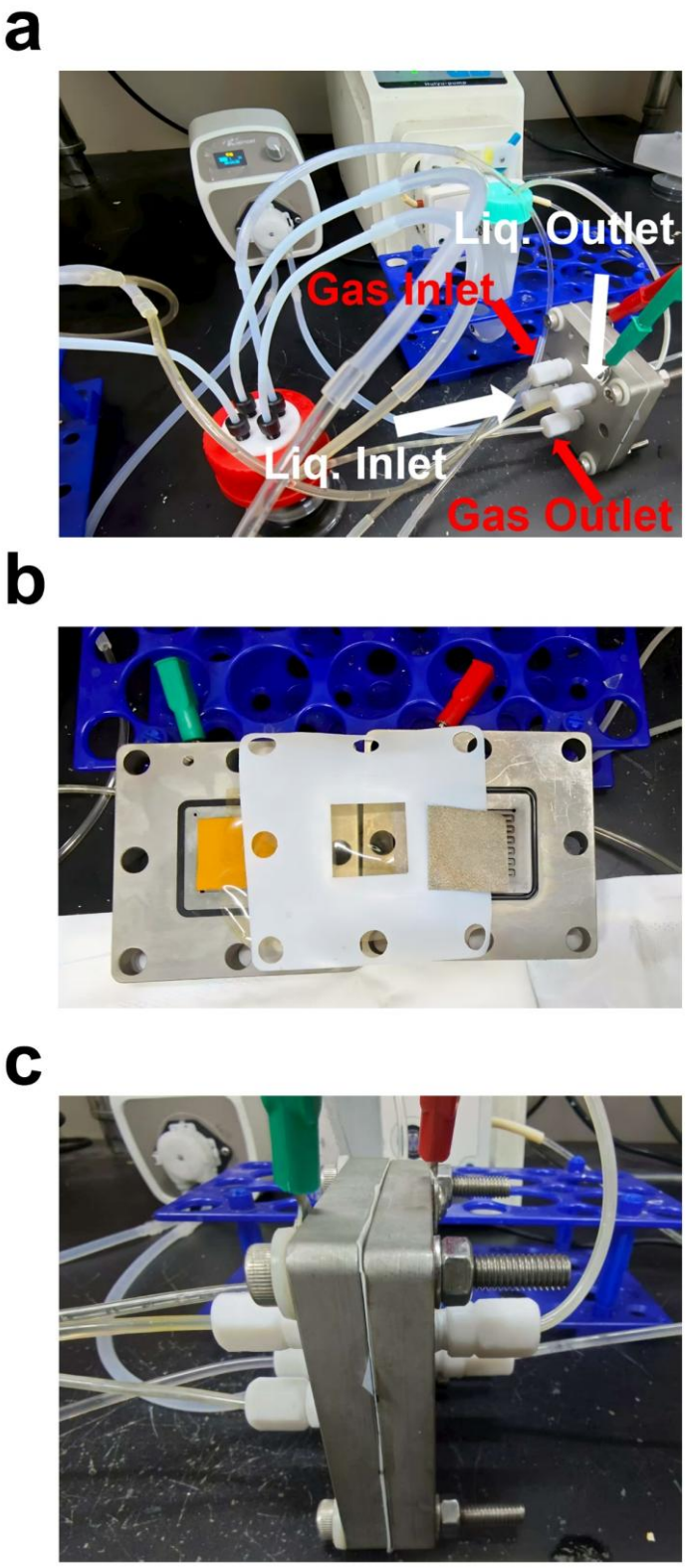

Fig. S3 The optical image of the modified zero-gap CO electrolyzer with an additional inlet and outlet for the fluid at the cathode/membrane interface from (a) front, (b) exploded, and (c) side view. The additional inlet and outlet for dedicated deionized water flow are indicated by blue arrows.

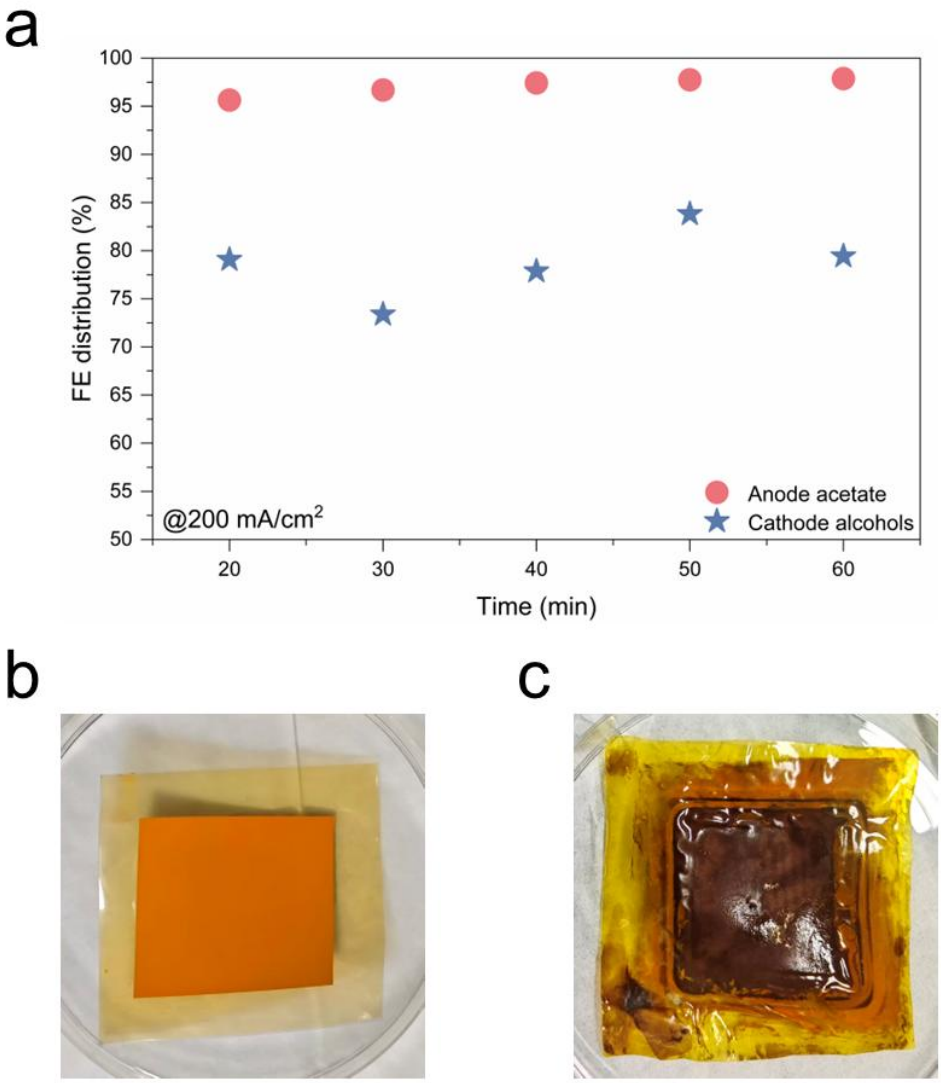

Fig. S4 (a) Faradaic efficiency distributions for anode acetate and cathode alcohols under direct catalyst-membrane (CCM assemblies) bonding conditions with extra fluid (FAA-3-50 membrane, 200 mA cm^{-2}). CCM before (b) and after (c) testing.

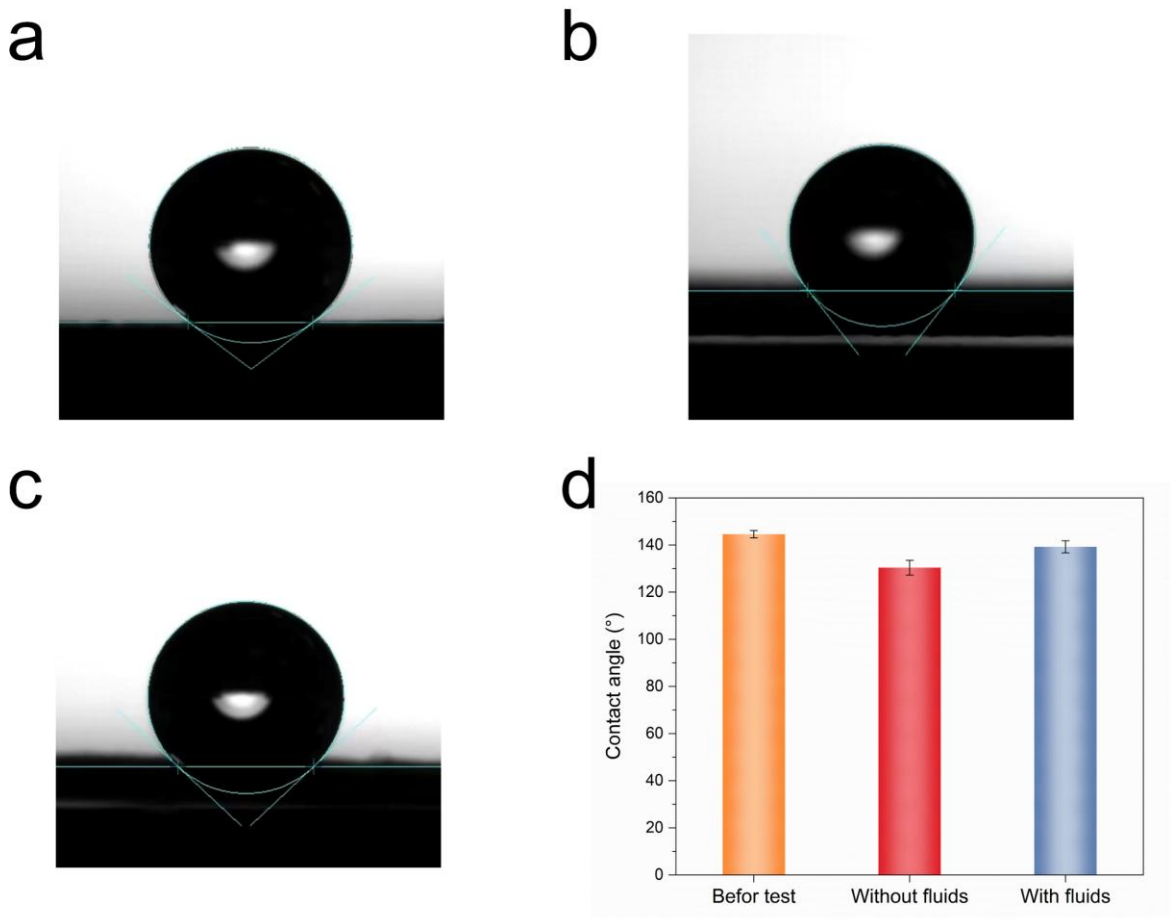

Fig. S5 (a-c) Photographs of water contact angles on the backsides of the gas diffusion layers: (a) before the test, (b) after the 1-h test without the extra fluid, (c) after the 1-h test with the extra fluids. (d) Comparison of the water contact angles in (a-c).

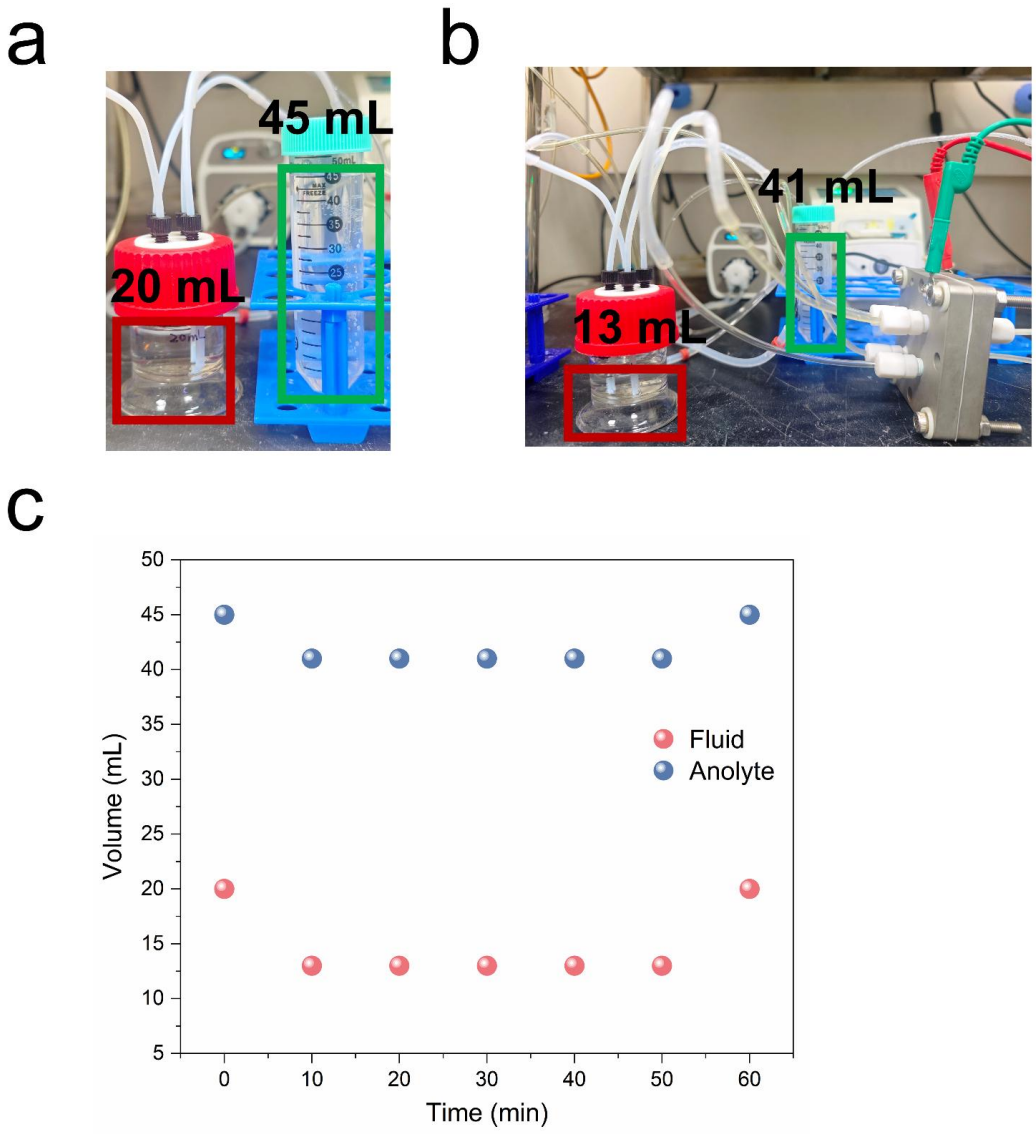

Fig. S6 (a and b) Photographs of the fluid and KOH anolyte before and during the test. (c) The volumes of the fluid and anolyte during the 1-h CO electroreduction measurement.

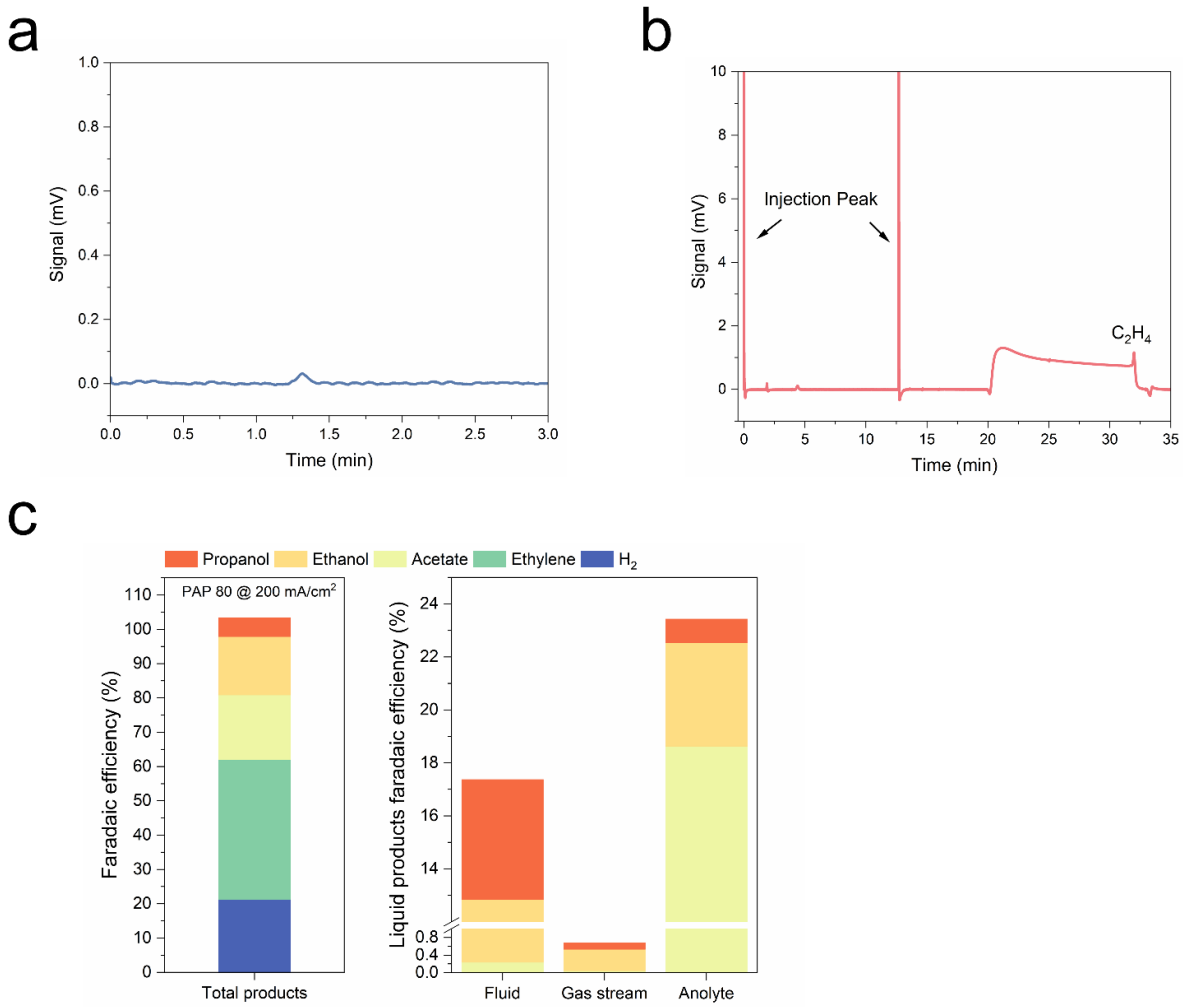

Fig. S7 (a and b) The raw gas chromatography results obtained using the sample collected from the headspace of the pure-water reservoir. (c) The total Faradaic efficiency and the breakdown analysis presenting the liquid product distribution in the fluid, the gas stream, and the anolyte.

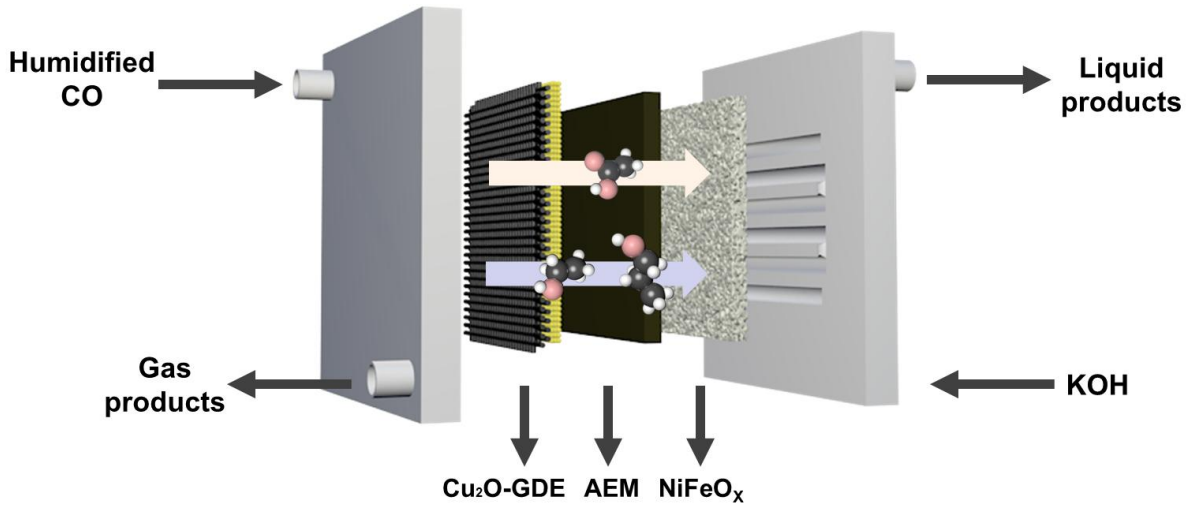

Fig. S8 Schematic illustrations of CO electrolyzers without the fluid.

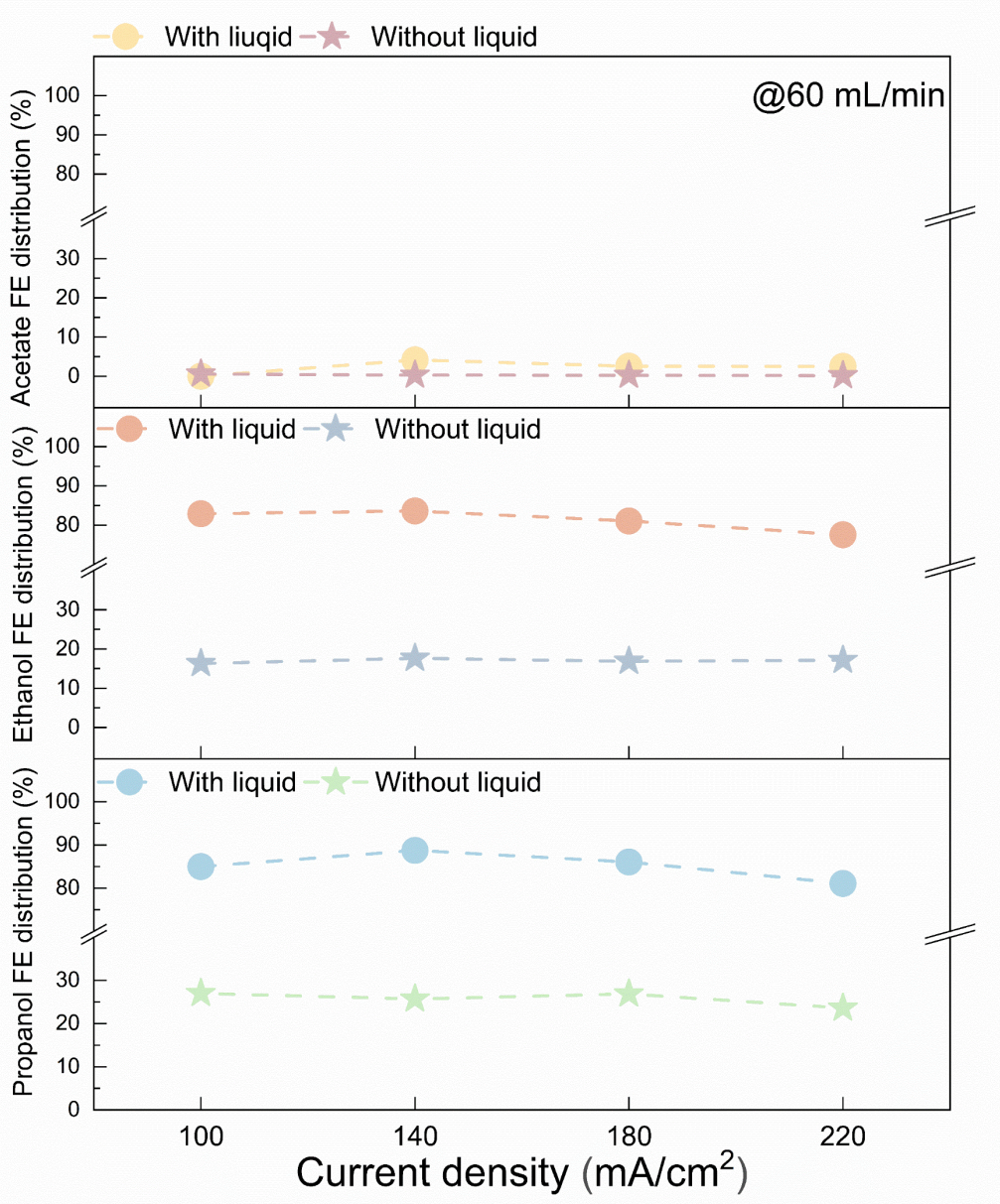

Fig. S9 The distribution of product FEs in regular electrolyzers (without liquid) and those with the fluid (with liquid) at the cathode.

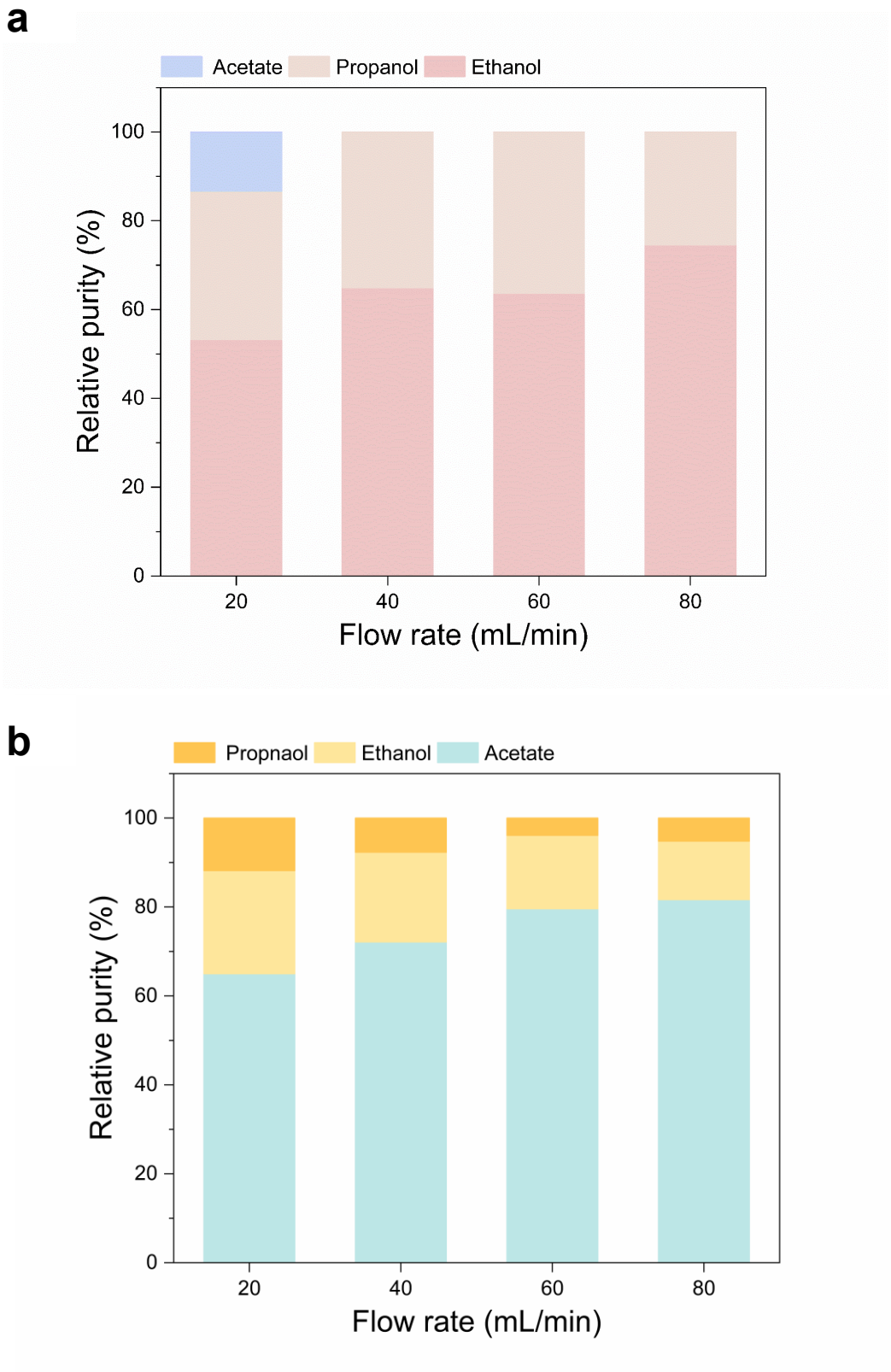

Fig. S10 Relative purities of products at the cathode (a) and anode (b) for CO reduction at varied flow rates and 100 mA cm^{-2}.

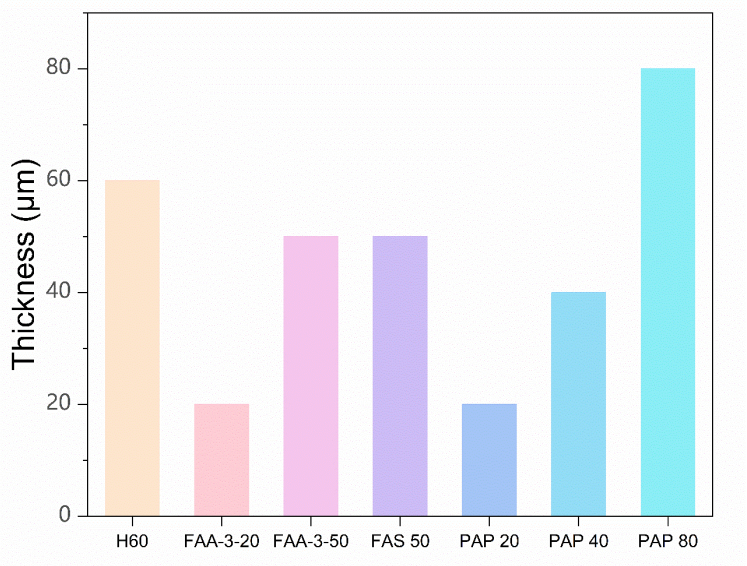

Fig. S11 Dry-state thicknesses of the seven anion-exchange membranes.

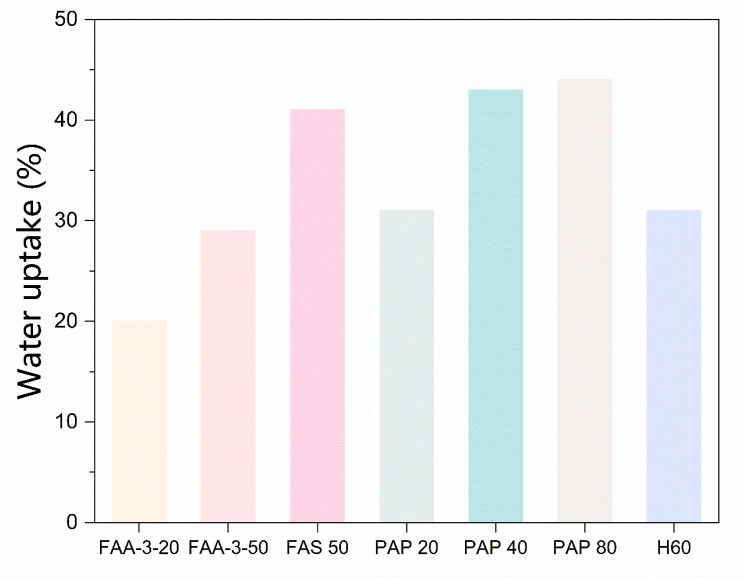

Fig. S12 Water uptake of the seven membranes.

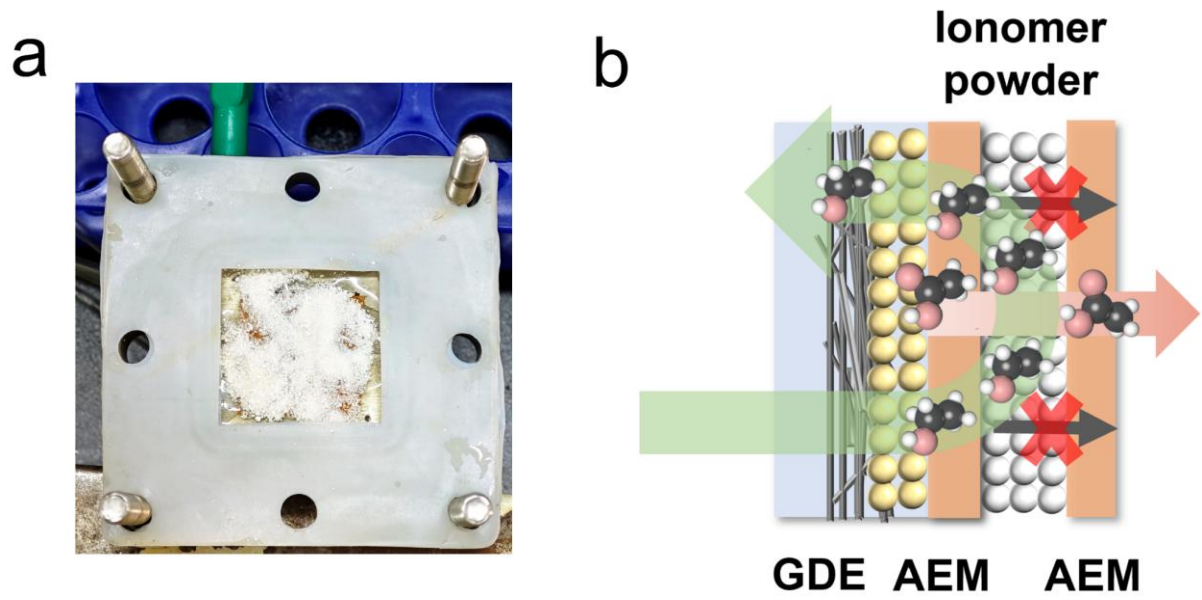

Fig. S13 (a) Photograph of the cell disassembled to show the interlayer consisting of ionomer powders and gaskets. (b) Schematic diagram of cell configuration with a controllable fluid thickness.

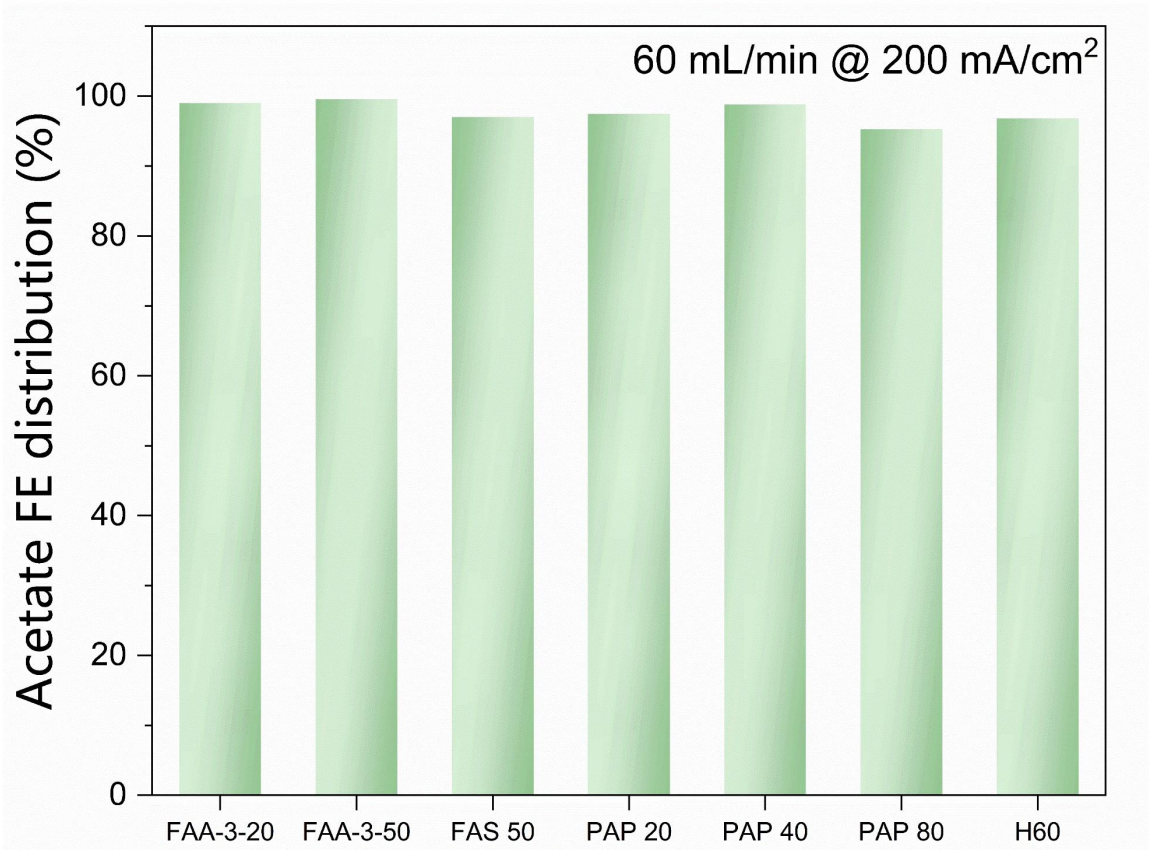

Fig. S14 Anode acetate FE contributions across the tested membranes.

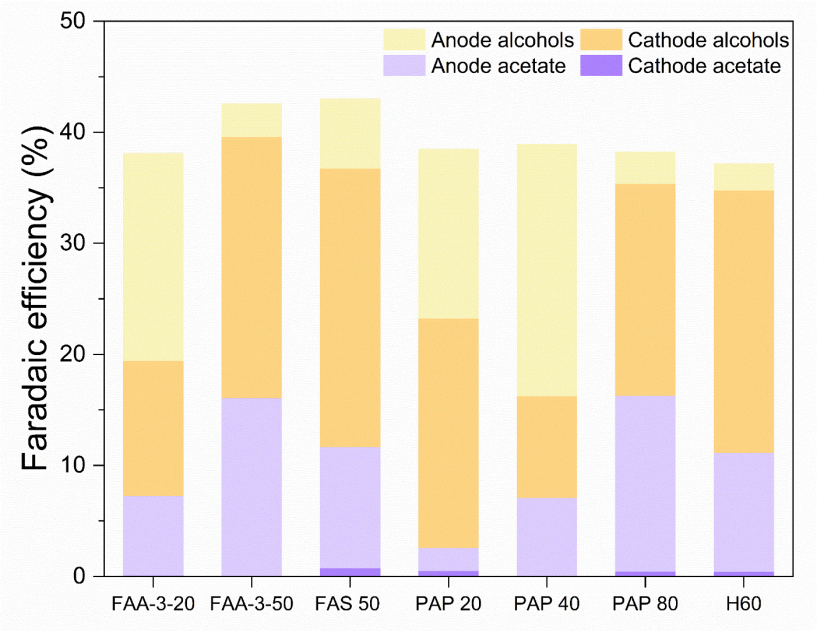

Fig. S15 Membrane-dependent product distribution. Faradaic efficiencies (FEs) of acetate and alcohols (ethanol and propanol) at the cathode and anode for the seven commercially available membranes.

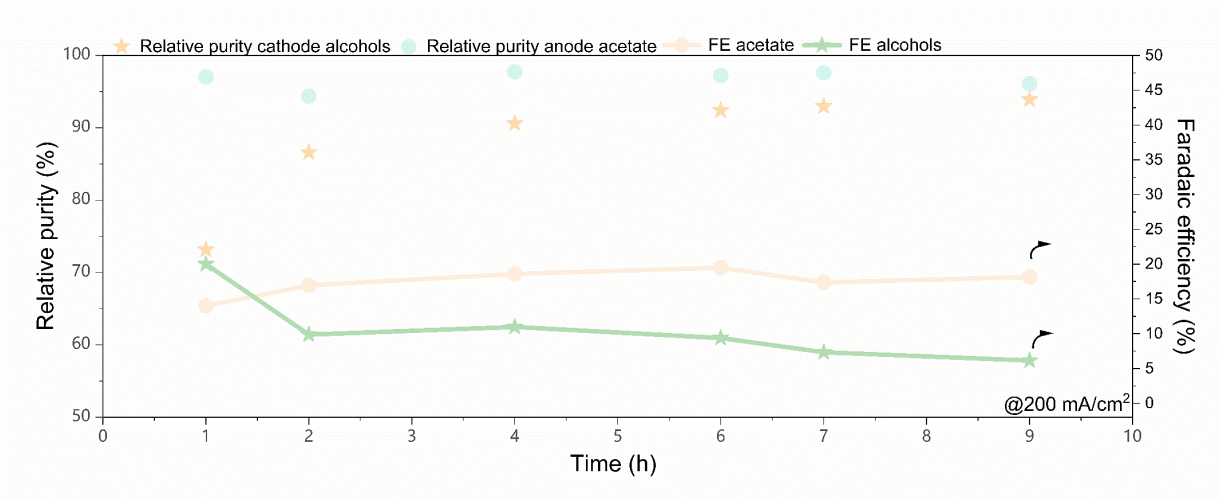

Fig. S16 Continuous CO electrolysis with the fluid at the cathode/membrane interface. FEs of oxygenates and relative product purities at the cathode and anode for FAA-3-50 membranes.

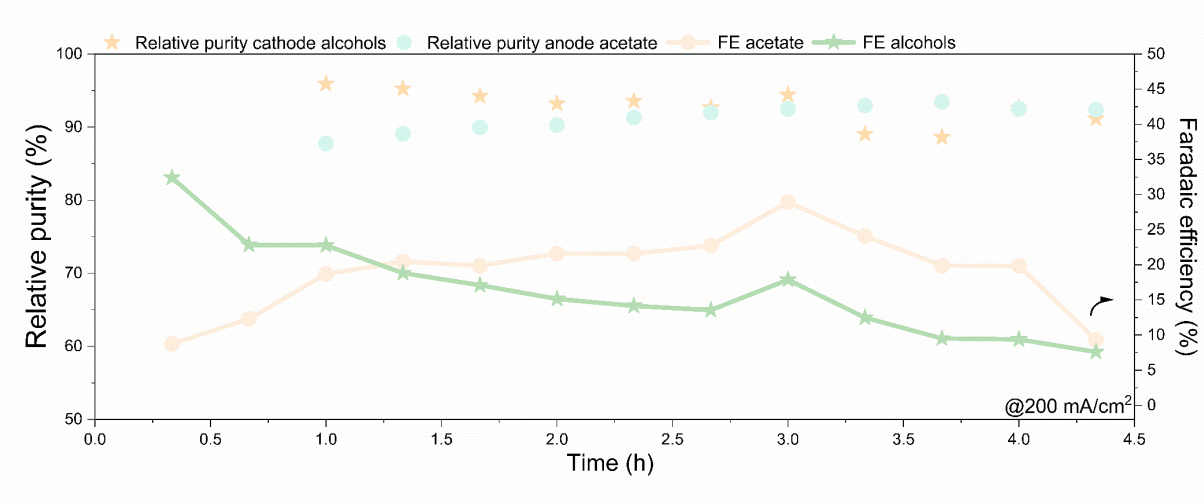

Fig. S17 Continuous CO electrolysis with the fluid at the cathode/membrane interface. FEs of oxygenates and relative product purities at the cathode and anode for PAP 80 membranes.

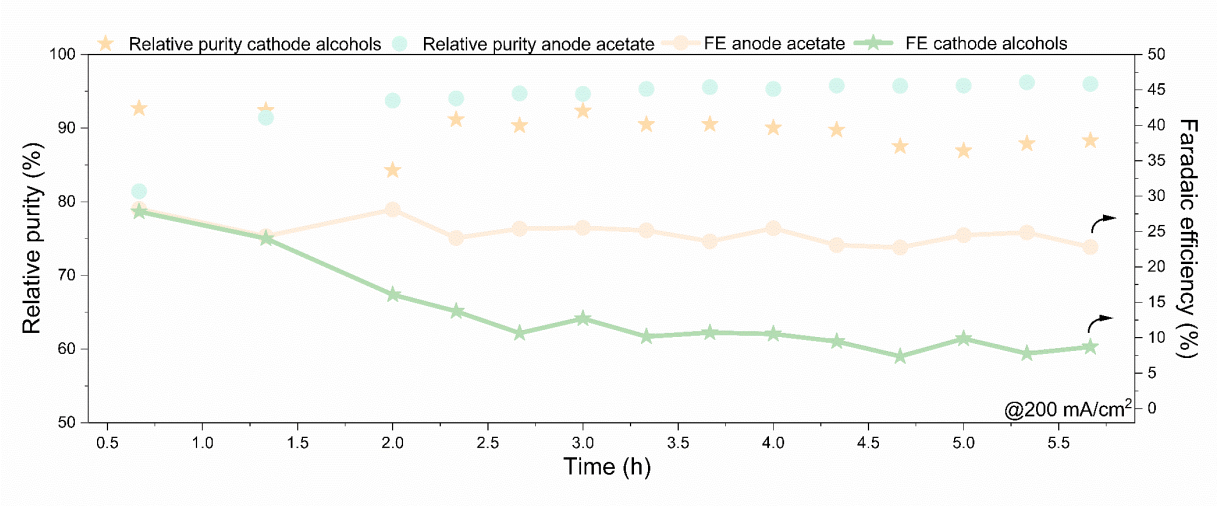

Fig. S18 Continuous CO electrolysis with the fluid at the cathode/membrane interface. FEs of oxygenates and relative product purities at the cathode and anode for H60 membranes.

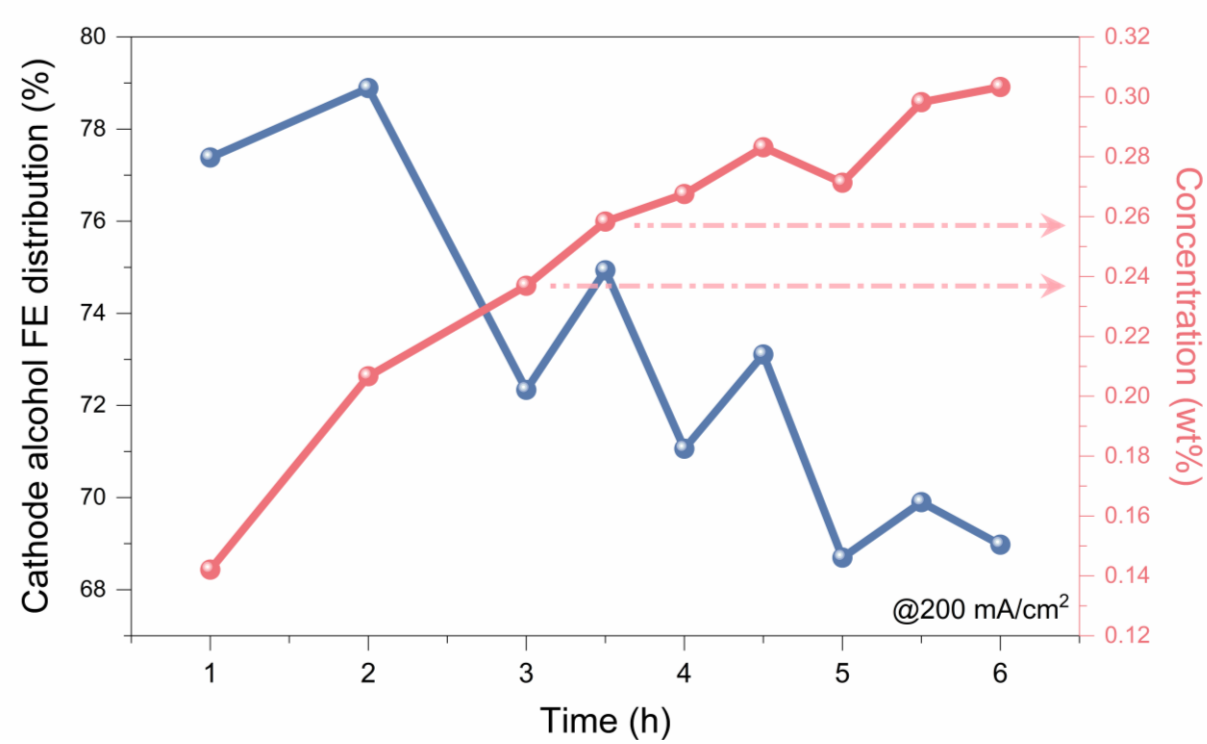

Fig. S19 Alcohol distribution in 6-h electrolysis. Cathode alcohol FE distribution (blue line, left axis) declines sharply as alcohol concentration (red line, right axis) surpasses the ~0.23 wt% threshold (dashed vertical line). Data obtained with the FAA-3-50 membrane at 100 mA cm^{-2} without fluid refreshment.

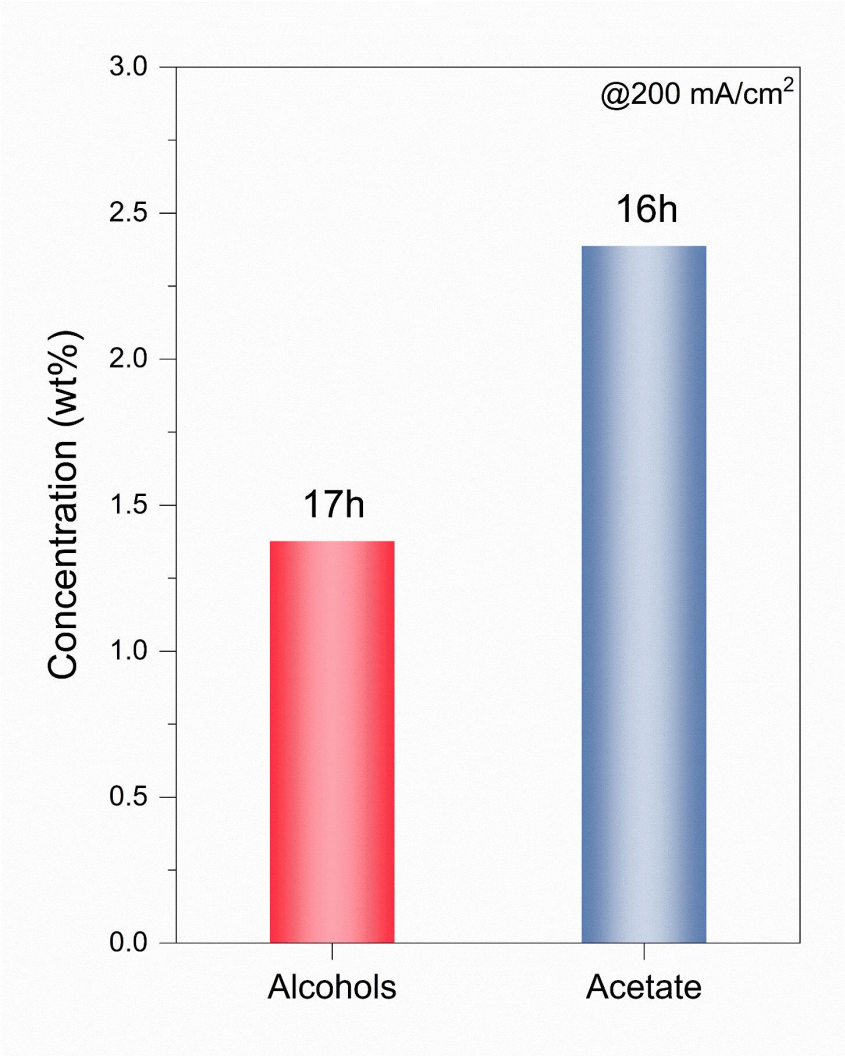

Fig. S20 Comparison of maximum acetate (PAP 20 membrane, 16 hours) and alcohol (FAA-3-50 membrane, 17 hours) concentrations achieved using different membranes.

Supporting Notes

Electrolyzer Assembly and Internal Configuration

This section provides a step-by-step visual guide to the electrolyzer hardware used in this study. The following notes detail the internal structure, component assembly, and key design features of the custom zero-gap cell employed for cathodic interface fluid management. Images and schematics illustrate how the fluid channels are integrated separately from gas pathways, ensuring distinct transport routes while maintaining catalyst–membrane contact.

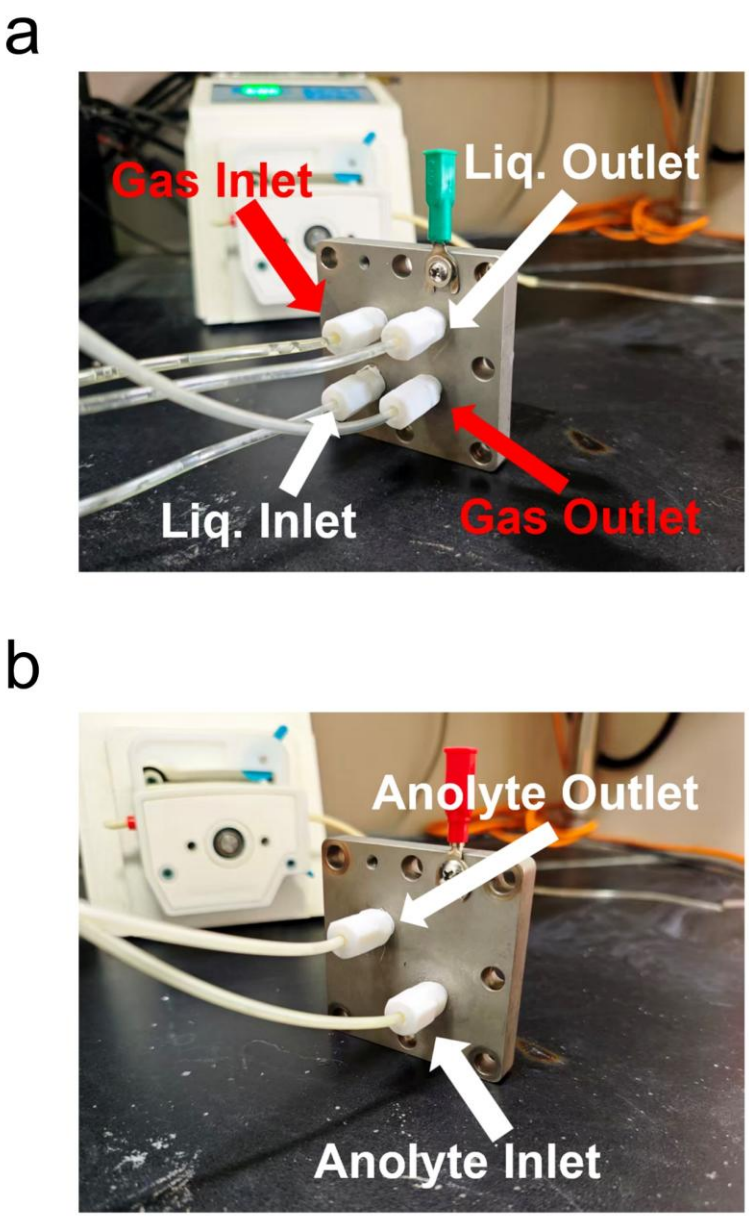

Fig. S21 Front view of the (a) cathode and (b) anode plate.

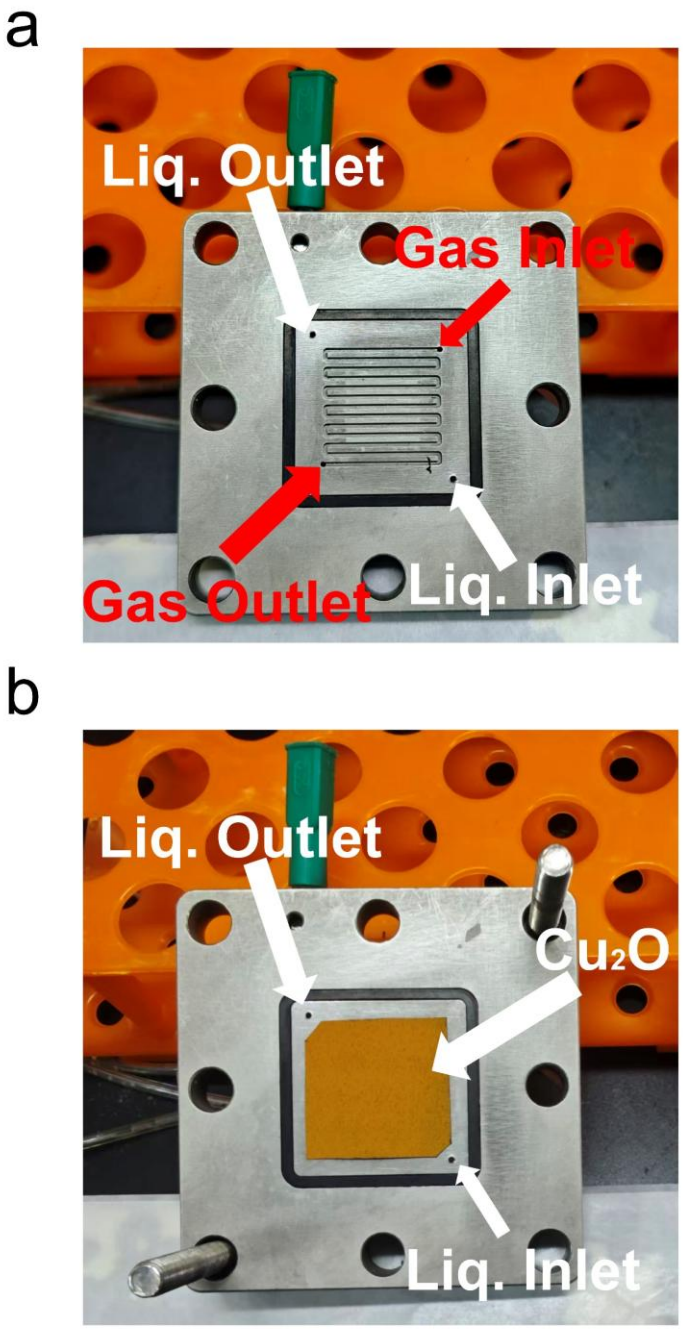

Step 1. The cathode plate shows the backside with machined gas channels and dedicated liquid ports. The cathode GDE (Cu_2O-coated carbon paper) is cut to fully cover the gas channels while leaving the liquid ports exposed.

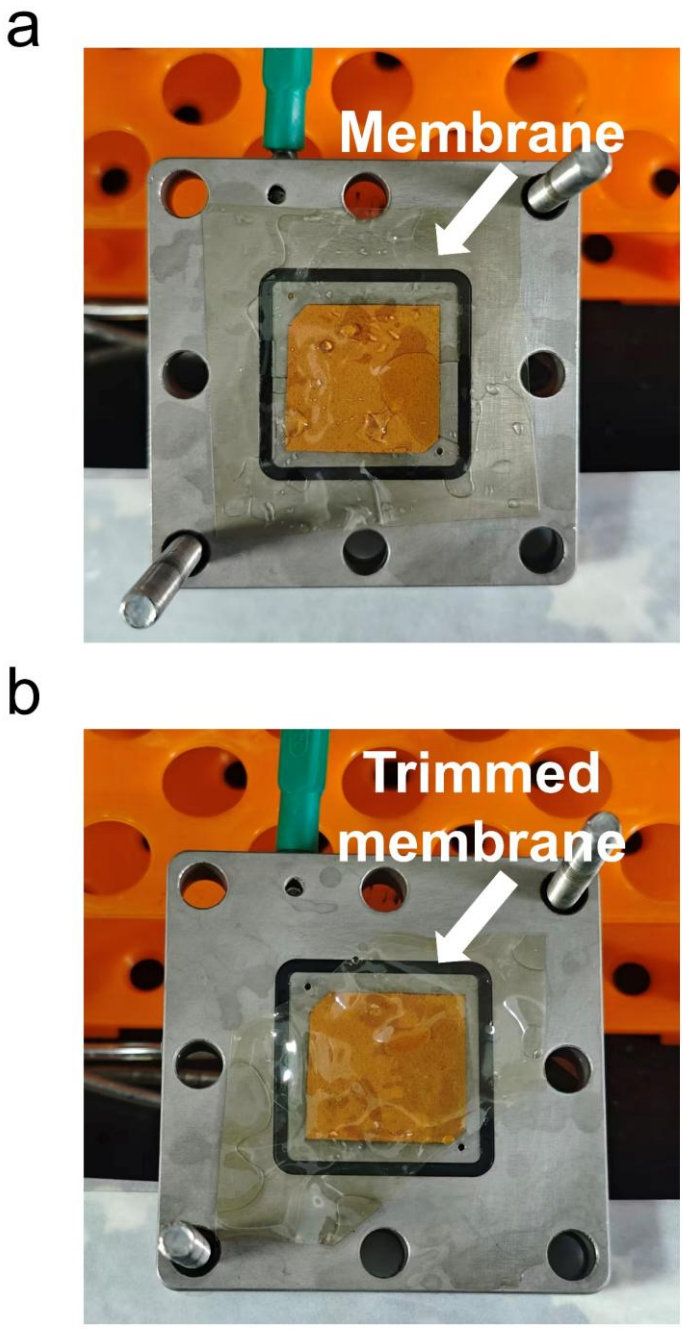

Step 2. An anion-exchange membrane is placed onto the electrode. For measurements without adding ionomer powders, a regular membrane is used, and Step 3 is skipped. For experiments with the ionomer powder interlayer, the membrane is cut to align with the liquid ports.

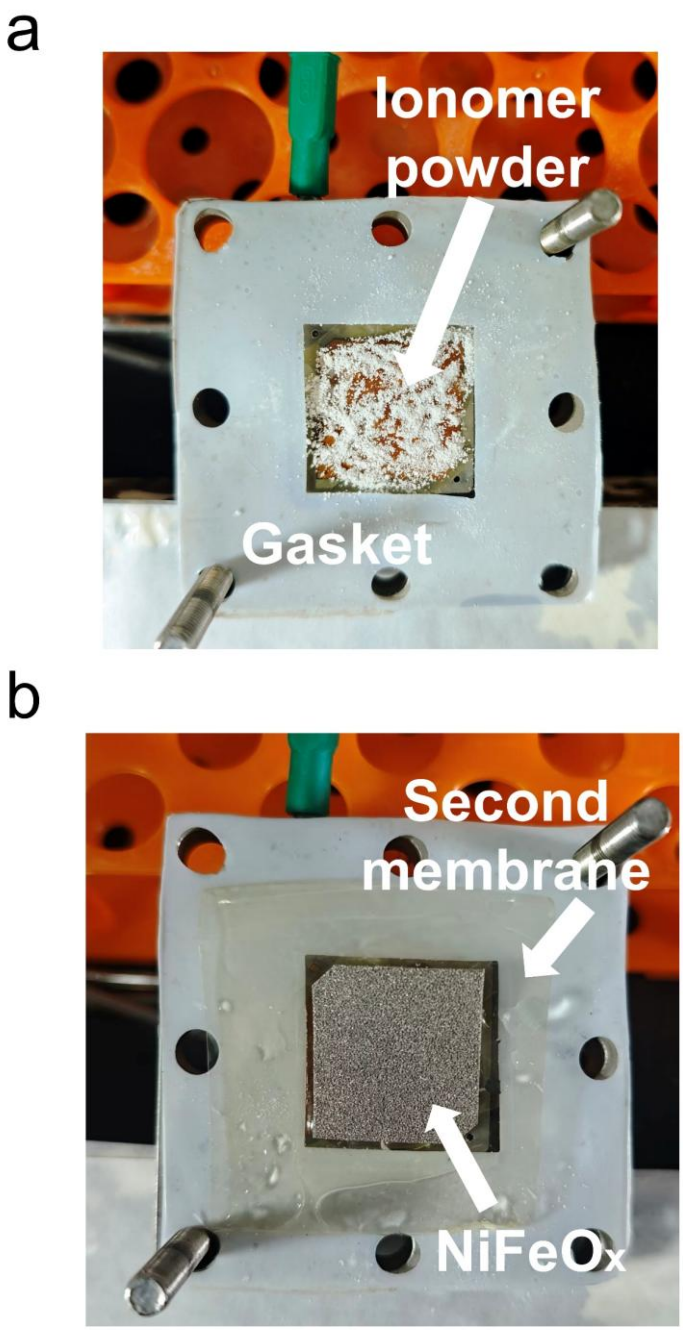

Step 3. The ionomer powder and gasket are applied to control the fluid thickness (h_{eff}), followed by placing a second membrane layer and a $NiFeO_x$ anode.

a

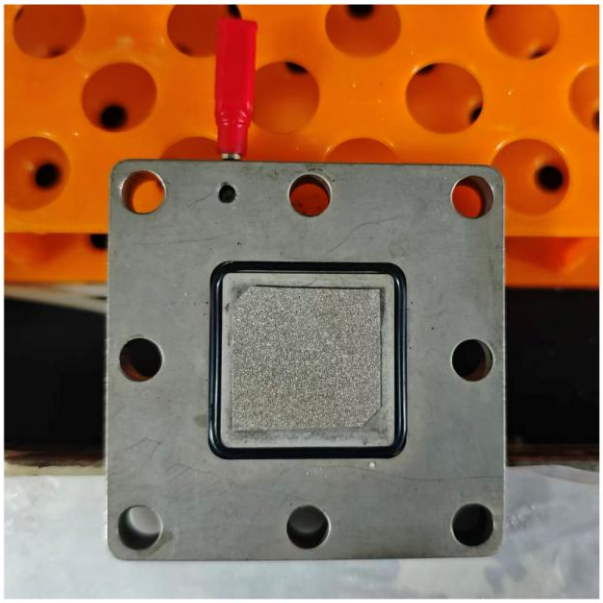

b

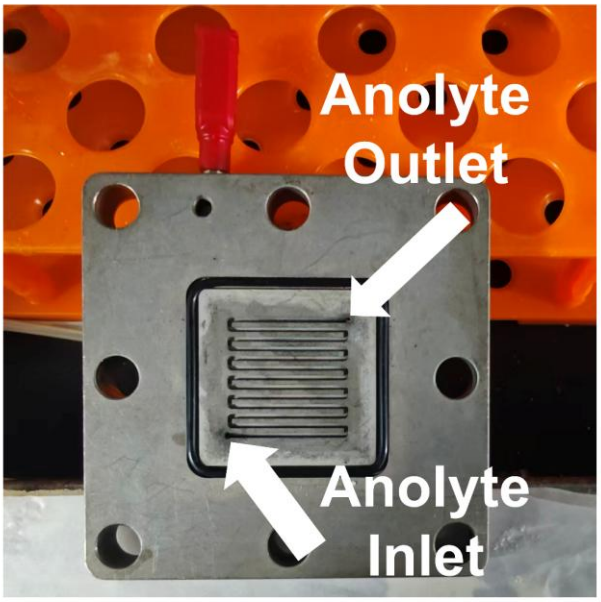

Step 4. The anode electrode ($NiFeO_x$) and the anode plate are applied to close the cell.